

# How to Perform Distributed Precoding to Wirelessly Power Shelf Labels: Signal Processing and Measurements

Gilles Callebaut, Jarne Van Mulders, Bert Cox, Liesbet Van der Perre, Lieven De Strycker, François Rottenberg  
*Department of Electrical Engineering, KU Leuven, Belgium*

**Abstract**—Wireless power transfer (WPT) has garnered increasing attention due to its potential to eliminate device-side batteries. With the advent of (distributed) multiple-input multiple-output (MIMO), radio frequency (RF) WPT has become feasible over extended distances. This study focuses on optimizing the energy delivery to Energy Receivers (ERs) while minimizing system total transmit power. Rather than continuous power delivery, we optimize the precoding weights within specified time slots to meet the energy requirements of the ERs. Both unsynchronized (non-coherent) and synchronized (coherent) systems are evaluated. Our analysis indicates that augmenting the number of antennas and transitioning from an unsynchronized to a synchronized full phase-coherent system substantially enhances system performance. This optimization ensures precise energy delivery, reducing overshoots and overall energy consumption. Experimental validation was conducted using a testbed with 84 antennas, validating the trends observed in our numerical simulations.

**Index Terms**—distributed MIMO, energy reduction, wireless power transfer

## I. INTRODUCTION

In recent years, there has been a growing body of literature focusing on wireless power transfer (WPT), covering both radio frequency (RF) and hardware solutions [2–4], as well as communication, signal, and system designs [5, 6]. Despite the significant efforts dedicated to the engineering of energy harvesters, as highlighted in [7] and illustrated in [8], there has been comparatively less emphasis on the co-design of signal and circuit-level, taking into account inherent nonlinear characteristics of WPT systems.

Several notable studies have explored different aspects of WPT optimization. For instance, [9] investigates the Pareto boundary, aiming for weighted-sum-power maximization (WSPMax) under fixed total transmit power constraints. Similarly, [10] focuses on increasing the output DC power by jointly optimizing multi-sine waveforms and beamforming, accounting for rectenna nonlinearity. The work presented in [11] delves into waveform design considering non-linear high-power amplifiers (HPA) and energy harvester (EH) non-linearities. Additionally, an overview of simultaneous wireless information and power transfer (SWIPT) is presented in [12].

The work is supported by the REINDEER project under grant agreement No. 101013425.

This paper is accepted at IEEE 25th International Workshop on Signal Processing Advances in Wireless Communications (IEEE SPAWC 2024) and can be found in [1].

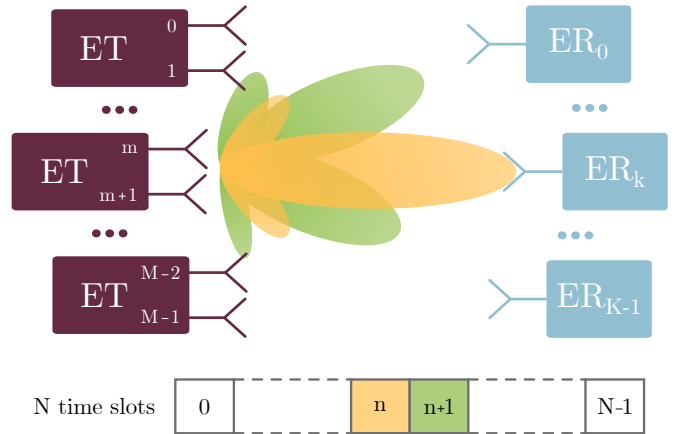


Fig. 1: Illustration of a distributed WPT system, where several Energy Transmitters (ETs) transmit signals over  $M$  antennas to  $K$  ERs to charge them over  $N$  time slots. In this example, during slot  $n$  only ER  $k$  is targeted, while at  $n + 1$  ER<sub>0</sub> and ER <sub>$K-1$</sub>  is being charged.

Contrary to prior research, we recognize that Energy Receivers (ERs) have distinct energy needs. For instance, electronic shelf labels (ESLs) may only require intermittent screen updates, eliminating the need for a continuous direct current (DC) power supply. As a result, instead of maximizing the received DC power for all ERs, our approach prioritizes delivering the essential energy to each ER with the least system transmit power.

We begin by introducing the system model, encompassing the RF-to-DC conversion model and the underlying assumptions of this study. In Section III, we formalize the problem for both non-coherent and coherent systems. The specific scenario under consideration is detailed in Section IV-A. We then proceed to evaluate the problem optimization through numerical and experimental assessments in Section V. Finally, we conclude with a summary and offer insights into future research directions in Section VI.

## II. SYSTEM MODEL

Consider a multi-antenna system as illustrated in Fig. 1, where  $M$  antennas are available to wirelessly charge  $K$  ERs. In the system model, we do not impose how these antennas are distributed, i.e., distributed or co-located. The received RF

power  $P_{\text{RF}}$  is converted to DC power  $P_{\text{DC}}$  by the harvester in the ER. The utilized RF-to-DC model is,

$$P_{\text{DC}} = \alpha P_{\text{RF}} - \beta, \quad (1)$$

where  $\alpha$  and  $\beta$  are real positive coefficient, and  $\alpha$  is the RF harvester efficiency and  $\beta$  is the minimum received RF power required to provide a stable voltage level to the ER circuitry. See Section IV-B for more details regarding the RF-to-DC power behavior.

Over  $N$  time slots, each lasting  $T$  seconds, the objective is to harvest a certain amount of energy  $E$  at each ER. The  $M$  antennas can be hosted on one (co-located system) or several (distributed system) ETs. An illustration of a distributed system with two antennas per ET is shown in Fig. 1. In this work, two scenarios are investigated, i.e., a non-coherent and a coherent scenario. In both scenarios, each antenna transmits the same narrowband signal. As opposed to communication signals, this signal carries only energy, not information. Hence, the transmitted signal is the same for all ERs.

*Assumptions.* Below is a list of assumptions used throughout the manuscript.

**(A1)** Although specified in some frequency bands, here no duty cycle limits are assumed during transmission. **(A2)** The power amplifiers (PAs) are presupposed to work in the linear regime. This can be obtained by employing a sufficient back-off or using techniques such as digital pre-distortion (DPD). **(A3)** The channel is considered static over the  $NT$  time period. Based on the findings [13, Fig. 1], this can be considered reasonable when both the ETs and ERs are static.

*Specific to the non-coherent system:* **(A4)** An independently and identically distributed (i.i.d.) phase difference is assumed for all received signals. This can be assumed when having different multipath components (MPCs) and, additionally, the transmit antennas each use different transmit phases. Additionally, **(A5)** the channel gain, i.e., path loss (PL), is perfectly known.

*Specific to the coherent system:* **(A6)** perfect channel state information (CSI) and **(A7)** perfect synchronization is assumed.

### III. OPTIMAL DISTRIBUTED PRECODING AND SWEEPING

Below, we formalize the problem of charging  $K$  ERs with  $M$  antennas in two scenarios. The symbols used are summarized in Table I.<sup>1</sup>

#### A. Non-Coherent System

Under (A4), on average, the received RF power is equal to the sum of all powers. Hence, using Eq. (1), the harvested DC power  $\tilde{p}_{k,n}$  at ER  $k$  at time slot  $n$  is *on average*<sup>2</sup>,

$$\tilde{p}_{k,n} = \alpha \sum_{m=1}^M (|h_{m,k}|^2 p_{m,n}) - \beta,$$

<sup>1</sup>The mathematical notations are detailed in <https://github.com/wavecore-research/math-notations>

<sup>2</sup>Here, by average we mean the expectation computed with respect to the i.i.d. phase distribution.

where  $p_{m,n}$  is the transmit power of antenna  $m$  at time slot  $n$  and  $h_{m,k}$  the complex channel coefficient between antenna  $m$  and ER  $k$ , which are known (A5). To minimize the total transmit energy while providing the required DC energy, the problem can be written as,

$$\min_{p_{m,n}} \sum_n \sum_m T p_{m,n} \quad \text{s.t.} \quad T \sum_n \tilde{p}_{k,n} \geq E, \quad \forall k \quad (2)$$

$$p_{m,n} \leq P_{\text{max}}, \quad \forall m, n, \quad (3)$$

with as constrain that the received energy over all time slots should be at least  $E$  for each ER and the transmit power does not exceed the maximum power constraint.

#### B. Coherent System

In the fully coherent scenario, perfect CSI (A6) and perfect synchronization (A7) is assumed. Each antenna precodes the narrowband transmit signal by a beamformer weight. At each time slot  $n$ , the beamformer can be reconfigured to preferably send to a given (or set of given) ER(s), as illustrated in Fig. 1. Hence, the beamformer vector is assumed to depend on the time slot. The beamforming vector at time slot  $n$  is denoted by  $\mathbf{w}_n \in \mathbb{C}^{M \times 1}$ . Assuming the transmit signal has unit power<sup>3</sup>, the total transmit power at time slot  $n$  is  $\|\mathbf{w}_n\|^2$  constraint to  $P_{\text{max}}$ . As a cost function for designing the beamformer weights, we would like to minimize the total transmit energy over the  $n$  time slots

$$\min_{\mathbf{w}_0, \dots, \mathbf{w}_{N-1}} T \sum_{n=0}^{N-1} \|\mathbf{w}_n\|^2,$$

with as constraint, that the received energy over all time slots should be at least  $E$  for each ER. The received RF signal power at time slot  $n$  for ER  $k$  is,

$$p_{\text{RF}k,n} = |\mathbf{h}_k^T \mathbf{w}_n|^2. \quad (4)$$

Taking into the account the efficiency of the harvester Eq. (1), the optimization problem becomes,

$$\min_{\mathbf{w}_0, \dots, \mathbf{w}_{N-1}} \sum_{n=0}^{N-1} T \|\mathbf{w}_n\|^2$$

$$\text{s.t.} \quad \sum_{n=0}^{N-1} T \alpha |\mathbf{h}_k^T \mathbf{w}_n|^2 \geq E + NT\beta, \quad \forall k.$$

The cost function is convex (quadratic) but the inequality is not convex because of the sign of the inequality. Therefore, we can rewrite the constraint using

$$\sum_{n=0}^{N-1} T \alpha |\mathbf{h}_k^T \mathbf{w}_n|^2 = \sum_{n=0}^{N-1} T \alpha \mathbf{h}_k^T \mathbf{w}_n \mathbf{w}_n^H \mathbf{h}_k^* = \text{tr}[\mathbf{G}_k \mathbf{X}]$$

where we defined  $\mathbf{G}_k = \mathbf{h}_k^* \mathbf{h}_k^T$  and  $\mathbf{X} = \alpha T \sum_{n=0}^{N-1} \mathbf{w}_n \mathbf{w}_n^H \in \mathbb{C}^{M \times M}$ . By its definition,  $\mathbf{X}$  is positive semidefinite and has

<sup>3</sup>This in contrast to the non-coherent scenario, where the transmit power is not unit power, but  $p_{m,n}$ .

a rank less or equal to  $\min(M, N)$ . In practice, we can reasonably expect that, by design, a large number of time slots will be available so that  $N \geq M$  and hence, the rank of  $\mathbf{X}$  is only constrained by its dimension  $M$ . This makes sense, we would like not to constraint the optimization and have  $N$  at least as large as  $K$  to be able to sweep across each ER. If not useful, the time slots will not be used by the optimization and the precoding weights at those timeslots will be set to zero. We can also note that  $\text{tr}[\mathbf{X}] = \sum_{n=0}^{N-1} \alpha T \|\mathbf{w}_n\|^2$ . Hence, the optimization problem can be rewritten as a function of  $\mathbf{X}$

$$\min_{\mathbf{X} \succeq 0} \text{tr}[\mathbf{X}] \text{ s.t. } \text{tr}[\mathbf{G}_k \mathbf{X}] \geq E + NT\beta, \forall k. \quad (5)$$

Given that  $N \geq M$ , this already reduces the dimension of the optimization variables from  $NM$  to  $M^2$ . Moreover, the cost function and constraint have a linear form, which is convex. This together with positive semidefinite constraint  $\mathbf{X} \succeq 0$ , yields a standard semidefinite programming structure and can be optimized using conventional solvers.

Based on the optimal  $\mathbf{X}$ , we can find back  $\mathbf{w}_n$  using, e.g., the eigenvalue decomposition (EVD). Consider that  $\mathbf{Q}$  is a unitary matrix  $\in \mathbb{C}^{M \times M}$  containing eigenvectors of  $\mathbf{X}$  and  $\mathbf{\Lambda}$  is a diagonal matrix of size  $\in \mathbb{C}^{M \times M}$  containing eigenvalues of  $\mathbf{X}$ . Then, the precoding matrix  $\mathbf{W}$  can be found as,

$$\begin{aligned} \mathbf{X} &= \alpha T \mathbf{W} \mathbf{W}^H \\ &= \mathbf{Q} \mathbf{\Lambda} \mathbf{Q}^H \\ \mathbf{W} &= \frac{1}{\sqrt{\alpha T}} \mathbf{Q} \mathbf{\Lambda}^{1/2}, \end{aligned}$$

where  $\mathbf{\Lambda}^{1/2}$  denotes taking the square root of each diagonal element of  $\mathbf{\Lambda}$ . Only the  $S$  columns of  $\mathbf{W}$  are used, associated with the  $S$  non-zero eigenvalues. This can be interpreted as using only  $S$  out of  $N$  timeslots.

#### IV. SCENARIO DESCRIPTION FOR EVALUATION

The proposed optimal distributed precoding and power allocation scheme is evaluated based on a representative use case, i.e., a wirelessly charging electronic shelf labels (ESLs) in a grocery store. The system is evaluated both numerically and experimentally, where the used parameters and their default values are summarized in Table I. Unless stated otherwise, the default values are used.

TABLE I: Used parameters, symbols, and expressions with their default value and units.

Parameter	Symbol	Default value	Unit
Carrier frequency	$f_c$	0.917	GHz
Required energy per node	$E_k$	500	mJ
Number of time slots	$N$	$(1, \dots, N = M)$	
Number of antennas	$M$	$(1, \dots, 84)$	
Time per timeslot	$T$	-	s
Time period	$NT$	12	h
Number of ESLs	$K$	240	
RF-to-DC efficiency	$\alpha$	0.16	-
Min. req. received RF power	$\beta$	0.0158	mW
Max. power per antenna	$P_{\max}$	4000	mW

#### A. Scenario

For both numerical analysis and measurements, we focus on a single shopping aisle within a grocery store as the deployment scenario. A representation of this setup is shown in Fig. 2. In this configuration, two shopping racks flank a 4 m wide aisle, each rack extending 8.4 m in length. Five shelves, spaced evenly on the 2.1 m tall racks, hold the ESLs at a depth of 0.5 m. We employ  $K = 84$  transmit antennas to power  $M = 240$  ESLs. These transmit antennas are integrated into the ceiling, providing power to the ESLs. The antenna array comprises pairs of antennas evenly spread across the ceiling. The 84 antennas are grouped into sets of 2, consistent with the testbed described in Section V-B.

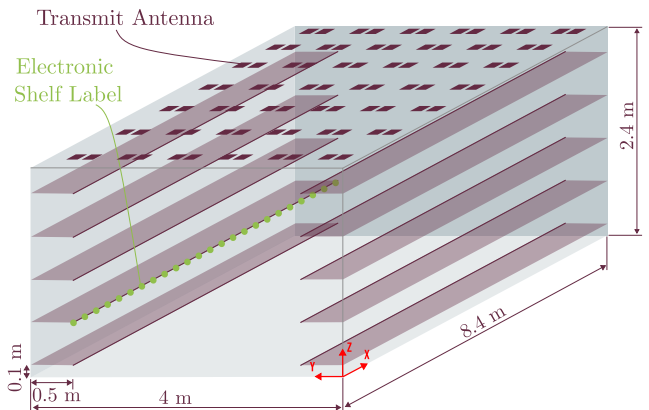


Fig. 2: Illustration of the Techtile testbed [14] simulating a supermarket aisle, featuring 84 ceiling-mounted antennas. The green circular areas indicate the placement of ESLs on a single shelf.

#### B. ESL Characterization

The system and the considered ESL operate at 917 MHz. In this band [15], a maximum transmit power of 4 W is permitted. The considered batteryless ESL device comprises an antenna, energy harvester, energy buffer, microcontroller, and an e-paper display. RF energy is captured by the antenna and converted to DC energy by the harvester IC. Once the energy buffer reaches the required level, the microcontroller initializes, receives downlink updates, and refreshes the e-paper display. The daily DC energy requirement is pivotal for our proposed optimization, influenced by the ESL's refresh rate and the energy needed for a screen update. The primary energy consumer in an ESL is the *E-Ink Raw Display*. As indicated in [16], updating the display consumes 450 mJ (30 mW over 15 s), with an additional 50 mJ required for Microcontroller Unit (MCU) operation and demodulating downlink signals. Thus, each ESL screen update demands 500 mJ. Given two updates daily, approximately 1 Ws/day/ESL is required. We consider the performance an RF energy harvesting test IC, designed to amplify and rectify low-input power levels to DC voltages. Its conversion efficiency,  $\alpha$ , and minimum required RF input power,  $\beta$ , are detailed in Table I, serving as key parameters in both numerical and experimental evaluations.

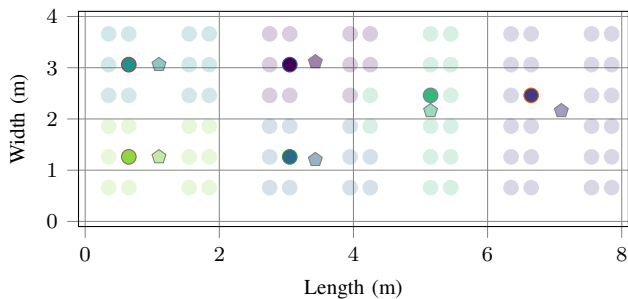


Fig. 3: Illustration of antenna selection method for different number of antennas. Dark dots represent the selected antennas, while the six pentagon markers indicate the centers of six clusters. The clusters are indicated by having the same colors. The clusters are determined by k-means clustering. The positions of non-selected antennas are shown with reduced transparency.


### C. Channel Model

We utilize the line-of-sight (LoS) *indoor factory* PL model of ETSI and 3GPP [17], which is suitable for environments with abundant metal, akin to the supermarket under consideration. We assume that the large-scale fading  $L_{m,k}$  does not change over the 12-hour window (A3) and is known at the antenna array (A5). The complex channel can then be modeled as  $h_{m,k} = \sqrt{L_{m,k}}e^{-j\phi_{m,k}}$ . The real positive coefficient  $L_{m,k}$  models the PL and is defined in [17]. A (uniform) random angle  $\phi_{m,k}$  is considered. Also, here, the channel is considered constant (A3) and known to the transmit antennas (A6).

### D. Antenna Selection Procedure

In the evaluation, the impact of increasing the number of antennas in the system is investigated. In order to have a fair comparison of the performance metrics for different number of antennas, the goal is to select a subset of antennas which are as evenly distributed as possible in the area (ceiling). To accomplish this, we designate a subset  $M_s$  ( $M_s = 0, \dots, |\mathcal{M}|$ ) from the available antennas  $\mathcal{M}$  using k-means clustering. We form  $M_s$  clusters, and then choose the antenna nearest to the center of each cluster. This selection process is depicted in Fig. 3.

## V. NUMERICAL AND EXPERIMENTAL EVALUATION

The optimization problems, Eq. (3) and Eq. (5), are solved using MOSEK and CVXPY in Python. The scripts are published in open-source, including additional figures [18] .

### A. Numerical Evaluation

The system's performance is assessed on its ability to deliver adequate energy to the devices without exceeding the required amount, aiming for precise energy delivery. Additionally, we analyze the total used average transmit power. This evaluation considers varying numbers of antenna elements and different system configurations (non-coherent vs. coherent).

1) *Impact on increasing the number of antennas:* Fig. 4 illustrates the required total transmit power of the entire system relative to the number of antennas utilized.<sup>4</sup> It can be observed that the performance of the non-coherent system plateaus quickly, whereas the coherent system shows improvement with an increasing number of antennas. The performance of the non-coherent system levels off around 10 antennas, with the optimization consistently utilizing only approximately 10 antennas regardless of the total number available. This in contrast to the coherent system, which utilizes all available antennas. **The optimization problem favors sparsity in the spatial (antenna) domain in the non-coherent case, which is not the case in the coherent system, where all antennas are utilized.**

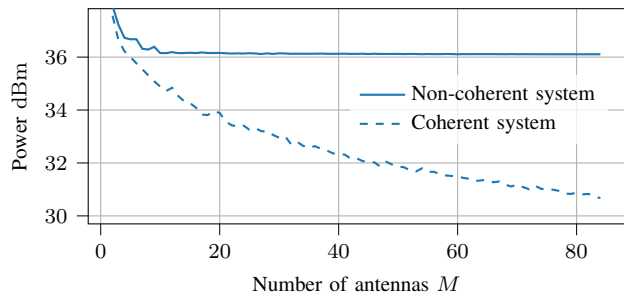


Fig. 4: Total transmit power of all deployed antennas for the coherent and non-coherent system. Initially, with a limited number of antennas, both systems exhibit similar transmit power, when the number of antennas increases, the non-coherent system plateaus, whereas the coherent system continues to improve.

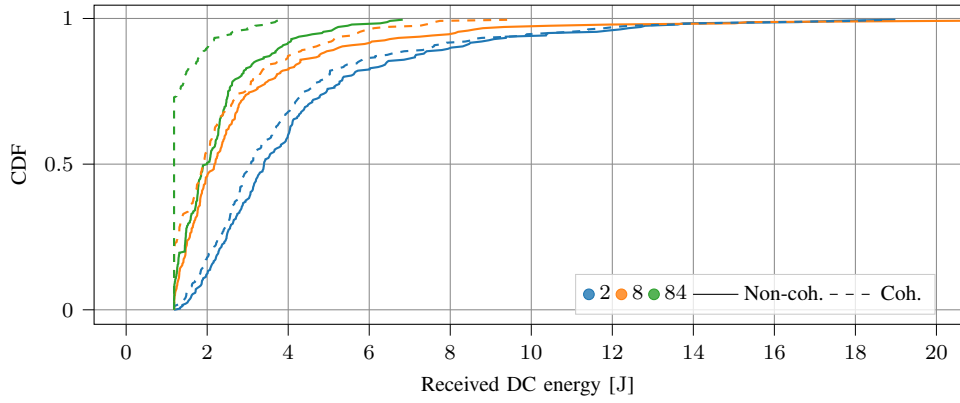
2) *Distribution of harvested energy:* In both systems, the accuracy of the targeted received DC power improves with having more antennas, as indicated by the cumulative distribution function (CDF) in Fig. 5a. With increased number of antennas, i) the total transmit power is decreased, ii) the variance of received energy over all ESLs is decreased and iii) the maximum received DC energy is reduced. The coherent system outperforms the non-coherent system in aforementioned regards, while at the same time uses less transmit power in Fig. 5a.

3) *Effect of number of timeslots:* In the non-coherent system, the solution keeps the same transmit power constant per antenna for all time slots and only uses a selection of the available antennas. This in contrast to the coherent, which utilizes only a few time slots and employs all antennas, as shown in Fig. 6. **In contrast to the spatial domain, in the temporal domain, the optimization problem favors sparsity in the coherent case, while using all time slots in the non-coherent system.**

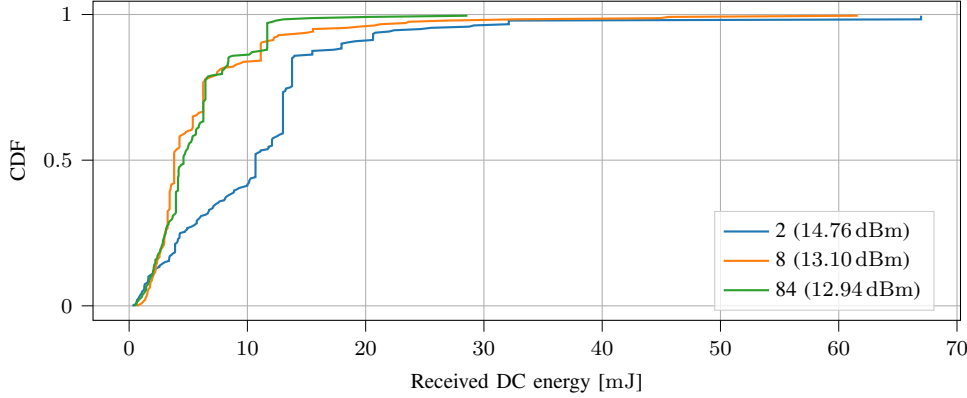
### B. Experimental Evaluation

The system setup, as introduced in Section IV-A and illustrated in Fig. 2, is emulated in the Tectile testbed [14] using all

<sup>4</sup>The power values should be interpreted as if the system were transmitting continuously at that level over the full 12 h period, although this is not the actual case, see Fig. 6.



(a) Numerical evaluation. CDF in the non-coherent (solid) and coherent (dashed) scenario.



(b) Experimental evaluation. Non-coherent measurements including the used total transmit power in brackets.

Fig. 5: Simulation (a) and measurement-based (b) CDF of the received DC energy over the full 12-hour window for 2, 8 and 84 antennas.

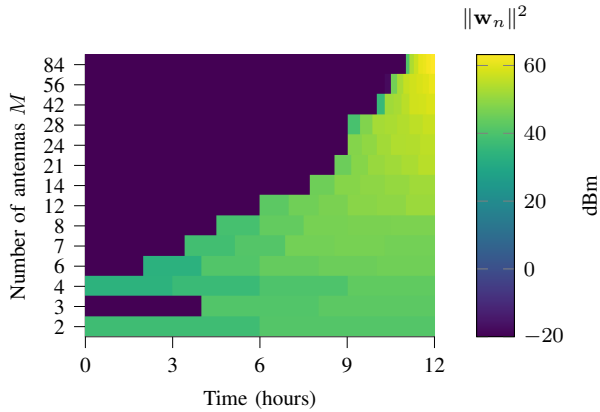


Fig. 6: The used transmit powers (z-axis) over the full-time window (x-axis) for different number of available antennas (y-axis) in the coherent system.

the 84 antennas on the ceiling. The experiment is conducted by using the results of the optimization problem in the non-coherent scenario, i.e., the power allocation per antenna. Measurements are performed at 917 MHz by collecting the average RF power at the ESL locations. The measured CDF of the received DC energy is plotted in Fig. 5b, where the DC energy is computed as  $E_k = \alpha p_{\text{RF}k} NT$ . The minimum received

power  $\beta$  is omitted, as the testbed has a lower maximum power (13.4 dBm) than required. Due to this limitation, the power allocations yielded by the optimization are scaled, i.e., 36 dBm becomes 13.4 dBm. The relative allocated transmit powers are hence kept the same. This yields thus the expected CDF, following the numerical evaluation, where the same trends can be observed, i.e., reduction of required transmit power, variance, and maximum received energy with increased number of available antennas.


## VI. CONCLUSIONS AND FUTURE OUTLOOK

We have defined the problem of wirelessly charging Energy Receivers (ERs) within a multi-antenna system, exploring both unsynchronized (non-coherent) and synchronized (coherent) configurations. Unlike previous approaches that aimed to maximize the total transferred energy, our focus was on minimizing the overall system transmit power while ensuring the required direct current (DC) energy supply. The analysis reveals that increasing the number of antennas and transitioning from an unsynchronized to a synchronized system significantly improve system performance. This enhancement ensures that the received energy aligns more closely with the system's requirements, eliminating overshoots and reducing overall energy consumption. Additionally, we evaluated the non-coherent system using a testbed equipped with 84 an-

tennas. The results obtained from this testbed corroborate the trends and observations identified in our numerical evaluations. Notable, providing a coherent system requires periodic calibration and additional signalling overhead in combination with higher hardware restrictions [14].

In future research, we aim to extend the minimization of total transmit power, to the total energy consumption of the system. Thereby also taking into account the energy related to the activation of Energy Transmitters (ETs). Additionally, investigating the impact of deviations from synchronization assumptions, including errors in synchronization and channel estimation, will be crucial. Integrating antenna patterns into the channel model will offer a more realistic representation of the system. We also intend to expand the scope of measurements for the coherent system and account for energy loss resulting from channel estimation. Lastly, considering linear power amplification without minimum power constraints may offer insights, as the current observations show very low power amplification values; including minimum constraints might encourage the use of more time slots.

#### REFERENCES

- [1] G. Callebaut, J. Van Mulders, B. Cox, L. Van der Perre, L. De Strycker, and F. Rottenberg, "How to Perform Distributed Precoding to Wirelessly Power Shelf Labels: Signal Processing and Measurements," in *2024 IEEE 25th International Workshop on Signal Processing Advances in Wireless Communications (SPAWC) (IEEE SPAWC 2024)*, Lucca, Italy, Sep. 2024, p. 4.97.
- [2] J. Huang, Y. Zhou, Z. Ning, and H. Gharavi, "Wireless Power Transfer and Energy Harvesting: Current Status and Future Prospects," *IEEE Wireless Communications*, vol. 26, no. 4, pp. 163–169, 2019.
- [3] M. Wagih, A. S. Weddell, and S. Beeby, "Rectennas for Radio-Frequency Energy Harvesting and Wireless Power Transfer: A Review of Antenna Design [Antenna Applications Corner]," *IEEE Antennas and Propagation Magazine*, vol. 62, no. 5, pp. 95–107, 2020.
- [4] J. Van Mulders *et al.*, "Wireless Power Transfer: Systems, Circuits, Standards, and Use Cases," *Sensors*, vol. 22, no. 15, 2022.
- [5] Y. Zeng, B. Clerckx, and R. Zhang, "Communications and Signals Design for Wireless Power Transmission," *IEEE Transactions on Communications*, vol. 65, no. 5, pp. 2264–2290, 2017.
- [6] B. Clerckx, K. Huang, L. R. Varshney, S. Ulukus, and M.-S. Alouini, "Wireless power transfer for future networks: Signal processing, machine learning, computing, and sensing," *IEEE Journal of Selected Topics in Signal Processing*, vol. 15, no. 5, pp. 1060–1094, 2021.
- [7] B. Clerckx, A. Costanzo, A. Georgiadis, and N. Borges Carvalho, "Toward 1G Mobile Power Networks: RF, Signal, and System Designs to Make Smart Objects Autonomous," *IEEE Microwave Magazine*, vol. 19, no. 6, pp. 69–82, 2018.
- [8] C. R. Valenta and G. D. Durgin, "Harvesting Wireless Power: Survey of Energy-Harvester Conversion Efficiency in Far-Field, Wireless Power Transfer Systems," *IEEE Microwave Magazine*, vol. 15, no. 4, pp. 108–120, 2014.
- [9] Y. Zeng, B. Clerckx, and R. Zhang, "Communications and Signals Design for Wireless Power Transmission," *IEEE Transactions on Communications*, vol. 65, no. 5, pp. 2264–2290, 2017.
- [10] S. Shen and B. Clerckx, "Joint Waveform and Beamforming Optimization for MIMO Wireless Power Transfer," *IEEE Transactions on Communications*, vol. 69, no. 8, pp. 5441–5455, 2021.
- [11] Y. Zhang and B. Clerckx, "Waveform Design for Wireless Power Transfer With Power Amplifier and Energy Harvester Non-Linearities," *IEEE Transactions on Signal Processing*, vol. 71, pp. 2638–2653, 2023.
- [12] B. Clerckx, R. Zhang, R. Schober, D. W. K. Ng, D. I. Kim, and H. V. Poor, "Fundamentals of Wireless Information and Power Transfer: From RF Energy Harvester Models to Signal and System Designs," *IEEE Journal on Selected Areas in Communications*, vol. 37, no. 1, pp. 4–33, 2019.
- [13] G. Callebaut, F. Rottenberg, L. V. der Perre, and E. G. Larsson, "Grant-Free Random Access of IoT devices in Massive MIMO with Partial CSI," in *2023 IEEE Wireless Communications and Networking Conference (WCNC)*, 2023, pp. 1–6.
- [14] G. Callebaut *et al.*, "Techtile – Open 6G R&D Testbed for Communication, Positioning, Sensing, WPT and Federated Learning," in *2022 Joint European Conference on Networks and Communications & 6G Summit (EuCNC/6G Summit)*, 2022, pp. 417–422.
- [15] European Telecommunications Standards Institute (ETSI), "EN 302 208," ETSI, ETSI Standard, Aug. 2020.
- [16] Waveshare. "2.9inch E-Paper (B) E-Ink Raw Display." (2023), [Online]. Available: <https://www.waveshare.com/2.9inch-e-Paper-B.htm> (visited on 2023).
- [17] ETSI, "5G; Study on channel model for frequencies from 0.5 to 100 GHz (3GPP TR 38.901 version 16.1.0 Release 16)," ETSI, Tech. Rep. TR 138 901 - V16.1.0 - 5G, 2020.
- [18] G. Callebaut and F. Rottenberg, *How to Perform Distributed Precoding to Wirelessly Power Shelf Labels: Signal Processing and Measurements*,  <https://github.com/wavecore-research/distributed-WPT-SPAWC2024>, 2024.